Geochemistry Geophysics Geosystems G3

Article
Volume 12, Number 5
17 May 2011
Q05007, doi:10.1029/2010GC003485
ISSN: 1525-2027

Published by AGU and the Geochemical Society

Potential causes for the non-Newtonian rheology of crystal-bearing magmas

Yolanda Deubelbeiss
Geophysical Fluid Dynamics, Institute of Geophysics, ETH Zurich, Sonneggstrasse 5, CH-8092 Zurich, Switzerland

Institute of Geochemistry and Petrology, ETH Zurich, Sonneggstrasse 5, CH-8092 Zurich, Switzerland

Now at WSL Institute for Snow and Avalanche Research SLF, Flüelastrasse 11, CH-7260 Davos Dorf, Switzerland

Boris J. P. Kaus
Geophysical Fluid Dynamics, Institute of Geophysics, ETH Zurich, Sonneggstrasse 5, CH-8092 Zurich, Switzerland (boris.kaus@erdw.ethz.ch)

Also at Department of Earth Sciences, University of Southern California, Los Angeles, California, USA

James A. D. Connolly
Institute of Geochemistry and Petrology, ETH Zurich, Sonneggstrasse 5, CH-8092 Zurich, Switzerland

Luca Caricchi
Department of Earth Sciences, University of Bristol, Wills Memorial Building, Bristol BS8 1RJ, UK

[1] Experimental studies indicate that crystal-bearing magma exhibits non-Newtonian behavior at high strain rates and solid fractions. We use a zero-dimensional (0-D) inversion model to reevaluate rheological parameters and shear heating effects from laboratory data on crystal-bearing magma. The results indicate non-Newtonian behavior with power law coefficients of up to $n = 13.5$. It has been speculated that finite strain effects, shear heating, power law melt rheology, or plasticity are responsible for this non-Newtonian behavior. We use 2-D direct numerical crystal-scale simulations to study the relative importance of these mechanisms. These simulations demonstrate that shear heating has little effect on aggregate (bulk) rheologies. Finite strain effects result in both strain weakening and hardening, but the resulting power law coefficient is modest (maximum $n = 1.3$). For simulations with spherical crystals the strain weakening and hardening behavior is related to rearrangement of crystals rather than strain rate related weakening. Finite strain effects were insignificant in a numerical simulation with naturally shaped crystals. Strain partitioning into the melt phase may induce microscopic stresses that are adequate to provoke a nonlinear viscous response in the melt. Large differential stresses and low effective stresses revealed by the simulations are sufficient to cause crystals to fail plastically. Numerical experiments that account for plastic failure show large power law coefficients ($n \approx 50$ in some simulations). We conclude that this effect is the dominant cause of the strong nonlinear viscous response of crystal-bearing magmas observed in laboratory experiments.

Components: 10,100 words, 14 figures, 2 tables.

Keywords: rheology; magma; crystals; numerical modeling.

Index Terms: 1236 Geodesy and Gravity: Rheology of the lithosphere and mantle (7218, 8160).

Received 28 December 2010; **Revised** 15 March 2011; **Accepted** 29 March 2011; **Published** 17 May 2011.

Deubelbeiss, Y., B. J. P. Kaus, J. A. D. Connolly, and L. Caricchi (2011), Potential causes for the non-Newtonian rheology of crystal-bearing magmas, *Geochem. Geophys. Geosyst.*, *12*, Q05007, doi:10.1029/2010GC003485.

1. Introduction

[2] The rheology of crystal-bearing magmas has been the subject of laboratory experiments and theoretical investigations (see e.g., *Stickel and Powell* [2005] and *Petford* [2009] for reviews). Pure, single-phase silicate melts are typically Newtonian, although they can be non-Newtonian at high strain rates [*Webb and Dingwell*, 1990a, 1990b]. However, the rheological behavior of crystal-bearing magmas, that is a suspension of crystals in melt, is often non-Newtonian and most commonly characterized by shear thinning behavior. Magmatic constitutive relations have been quantified in several studies [e.g., *Pinkerton and Stevenson*, 1992; *Lejeune and Richet*, 1995; *Costa*, 2005; *Caricchi et al.*, 2007; *Cordonnier et al.*, 2009; *Costa et al.*, 2009; *Petford*, 2009]. The majority of these studies focus on the estimation of macroscopic rheological parameters and provide limited insight into the underlying physics. A number of experimental studies have explored the influence of particle fraction [*Rutgers*, 1962; *Arzi*, 1978; *Lejeune and Richet*, 1995], and shape [*Cleary*, 2008; *Mueller et al.*, 2010]. *Champallier et al.* [2008] demonstrated that crystal suspensions in silicate melts may have a strongly nonlinear, shear thinning, viscous rheology. Analogue experiments also show nonlinear, shear thinning, rheology [*Mueller et al.*, 2010]; although in the analog experiments the nonlinearity is weak and sometimes manifest as a shear thickening effect. Non-Newtonian effects also occur in colloidal suspensions but they are attributed to effects that have been shown to be insignificant for silicate magmas [*Mueller et al.*, 2010]. The cause of the non-Newtonian rheology of magmas has not been resolved [e.g., *Cordonnier et al.*, 2009; *Mueller et al.*, 2010] and is the focus of this investigation.

[3] We employ a 0-D model to fit the full stress-strain curves of published laboratory experiments. This model allows us to extract the effective suspension viscosity as a function of strain rate, and to quantify the nonlinearity of the viscous component of the rheology. To elucidate the underlying causes for this nonlinearity we perform systematic 2-D numerical simulations, from which we extract stress-strain curves that are analyzed with the same 0-D model. The 2-D numerical simulations are performed on the spatial scale of individual particles assuming visco-elasto-plastic rheology. This method facilitates the analysis of microstructures as well as local stress, strain and strain rate distribution inside the crystal-melt system with evolving time. By controlling the melt and solid rheologies independently we can test the relative importance of shear heating, power law melt rheology, finite strain effects (microstructural reordering of crystals) and plasticity for the overall rheological behavior of the crystal-melt suspension. We also evaluate the effect of crystal shape on suspension rheology.

2. Zero-Dimensional Analysis of Laboratory Experiments

[4] The laboratory experiments of *Caricchi et al.* [2007] tested the strain rate dependence of rheology by performing so-called strain rate stepping experiments. In these experiments samples are deformed at a specified strain rate until the stress-strain rate curve flattens, at which point the strain rate is increased (Figure 1a). The effective viscosity (and hence the power law coefficient) can then be computed a posteriori from the 'flat' part of the stress-strain rate curve, while the initial phase reflects the influence of elastic rheology. Because graphical identification of the viscous component is subjective, we employ a 0-D Maxwell viscoelastic model to invert the entire stress-strain curve for the relevant rheological parameters This has the advantage that we simultaneously establish the effective elastic shear modulus and viscosity of the sample, and that we are able to obtain accurate viscosity estimates for experiments in which the stress-strain curves are not perfectly flat.

[5] Our 0-D Maxwell viscoelastic model is based on the same assumptions used in interpreting most laboratory experiments, namely that the bulk strain rate in the sample is homogeneous. Mathematically,

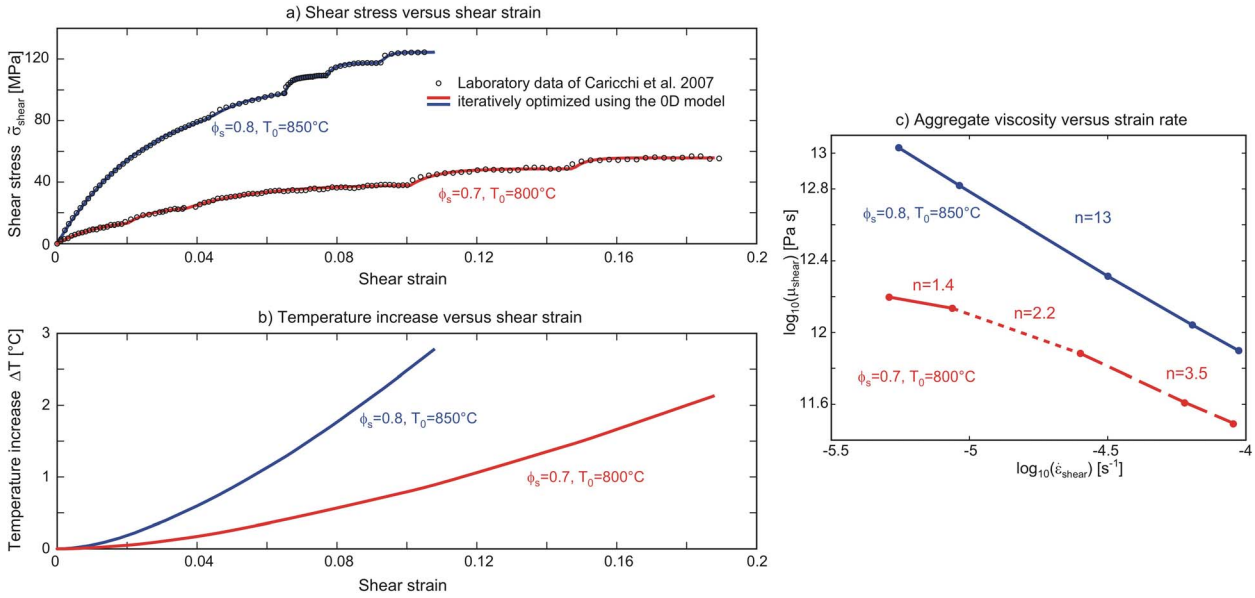

Figure 1. Two worked examples of fitting experimental data of a magma suspension containing crystals with a 0-D viscoelastic rheological model. (a) Laboratory-derived and numerically computed stress-strain curves for two different experiments. (b) Maximum amount of temperature increase due to shear heating. (c) Suspension viscosity as a function of strain rate on double logarithmic axes. The power law coefficients, computed from these curves, can reach large values.

this assumption implies [e.g., *Kaus and Podladchikov*, 2006]

$$\frac{\partial \sigma}{\partial t} = 2G\dot{\varepsilon} - \frac{G}{\mu}\sigma, \tag{1}$$

where G and μ are the effective shear modulus and viscosity, t is time, σ is stress and $\dot{\varepsilon}$ strain rate.

[6] We also compute the shear heating effect by assuming that the system is adiabatic (does not loose heat) in which case

$$\frac{\partial T}{\partial t} = \frac{\sigma}{\rho c_p}\left(\dot{\varepsilon} - \frac{1}{2G}\frac{\partial \sigma}{\partial t}\right), \tag{2}$$

where T is temperature, c_p heat capacity, and ρ is density. Equations (1) and (2) are coupled ordinary differential equations that are solved forward in time using the MATLAB ODE (ordinary differential equation) toolbox, where each simulation yields a stress-strain and a temperature curve. The best fit values of G and μ for a given strain rate are determined in an automated manner with a simplex search algorithm [*Lagarias et al.*, 1998], from which we in turn can compute the power law coefficient (see Figure 1 for two worked examples).

[7] It is instructive to study how the power law coefficient varies in laboratory experiments. For this purpose we reanalyzed the published experiments with our 0-D model. Results show a strong non-Newtonian behavior with power law coefficients of up to n = 13.5 (Figure 2). This is an extremely large value compared to most laboratory experiments on natural samples, which typically have power law exponents less than 5.

[8] There is nearly no correlation of n with crystal fraction and initial temperature. Yet, some correlation exists with maximum aggregate stress as well as with adiabatic temperature increase (Figures 2c and 2d), which suggests that shear heating or stress might play a role. As these results are inconclusive, we performed 2-D numerical simulations and analyze the stress-strain curves from these simulations with the same 0-D method.

3. Governing Equations, Numerical Method, and Model Setup

3.1. Rheological Model

[9] We assume 2-D incompressible Stokes flow of either linear or nonlinear viscous rheology. We further consider elastic and plastic deformation as well as shear (viscous) heating. The governing

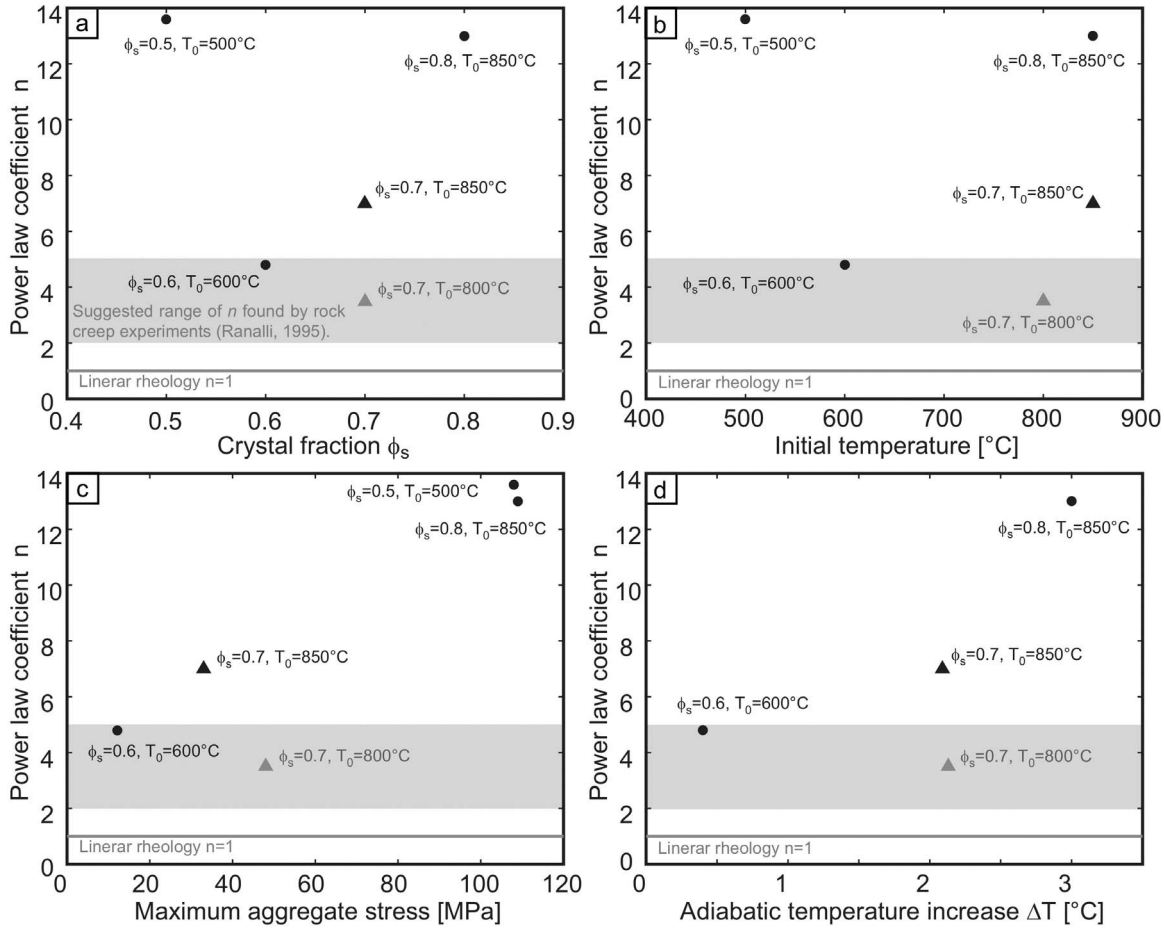

Figure 2. Power law coefficient computed from fitting the 0-D model to the laboratory experiments of *Caricchi et al.* [2007]. Results are plotted versus (a) crystal fraction, (b) initial sample temperature, (c) maximum obtained stress, and (d) adiabatic temperature increase. The gray bar indicates the range of power law coefficients for solid rock experiments. In some experiments, n increases with increasing strain rate (e.g., Figure 1c). In these cases we report n and the maximum aggregate (bulk) stress at $\dot{\varepsilon} = 3 \times 10^{-5}$ s^{-1}.

equations, written using Einstein summation convention, are as follows: conservation of mass

$$\frac{\partial v_i}{\partial x_i} = 0, \tag{3}$$

where v_i denotes velocity and x_i are spatial coordinates (i = 1, 2), and force balance

$$\frac{\partial \sigma_{ij}}{\partial x_j} = 0, \tag{4}$$

where σ_{ij} are total stresses. Total stress and strain rate are defined as

$$\sigma_{ij} = -P\delta_{ij} + \tilde{\sigma}_{ij}, \tag{5}$$

$$\dot{\varepsilon}_{ij} = \frac{1}{2}\left(\frac{\partial v_i}{\partial x_j} + \frac{\partial v_j}{\partial x_i}\right), \tag{6}$$

where $\tilde{\sigma}_{ij}$ denotes deviatoric stress, P pressure, δ_{ij} the Kronecker delta and $\dot{\varepsilon}_{ij}$ strain rate.

[10] We use a Maxwell visco-elasto-plastic rheology because it is the simplest rheology that is capable of describing the entire measured stress-strain curves, and simultaneously capable of simulating brittle failure. For this rheology, deviatoric deformation is described by

$$\dot{\varepsilon}_{ij} = \dot{\varepsilon}_{ij}^{vis} + \dot{\varepsilon}_{ij}^{el} + \dot{\varepsilon}_{ij}^{plast} = \frac{1}{2\mu_{eff}}\tau_{ij} + \frac{1}{2G}\frac{D\tilde{\sigma}_{ij}}{Dt} + \dot{\lambda}\frac{\partial Q}{\partial \sigma_{ij}}, \tag{7}$$

where $\dot{\varepsilon}_{ij}^{vis}$, $\dot{\varepsilon}_{ij}^{el}$ and $\dot{\varepsilon}_{ij}^{plast}$ are the elastic, viscous and plastic strain rates, respectively, G the elastic shear modulus, μ_{eff} viscosity, $\dot{\lambda}$ is a plastic multiplier and Q is the plastic flow potential [*Moresi et al.*, 2007;

Kaus, 2010]. The Jaumann objective derivative of the deviatoric stress tensor versus time is

$$\frac{D\tilde{\sigma}_{ij}}{Dt} = \frac{\partial \tilde{\sigma}_{ij}}{\partial t} + v_k \frac{\partial \tilde{\sigma}_{ij}}{\partial x_k} - W_{ik}\tilde{\sigma}_{kj} + \tilde{\sigma}_{ik}W_{kj}, \quad (8)$$

where $W_{ij} = \frac{1}{2}\left(\frac{\partial v_i}{\partial x_j} - \frac{\partial v_j}{\partial x_i}\right)$ is the vorticity. Laboratory experiments indicate that brittle failure of crystals may affect the rheology of the system [*Lavallée et al.*, 2007], which is approximated here by a nonassociated Mohr-Coulomb plasticity, where (in 2-D) the yield condition F and the plastic flow potential Q are given by

$$F = \tilde{\sigma}^* - \sigma^* \sin(\theta) - C\cos(\theta) \quad (9)$$

$$Q = \tilde{\sigma}^*, \quad (10)$$

where $\tilde{\sigma}^* = \sqrt{((\sigma_{xx} - \sigma_{zz})/2)^2 + \sigma_{xz}^2}$, $\sigma^* = -0.5(\sigma_{xx} + \sigma_{zz})$, C denotes cohesion, θ the friction angle, which in our model is assumed to be zero (because the magmatic fluid pressure is very large) so that plasticity arises entirely due to the cohesion criterion.

[11] Plastic deformation occurs if stresses are locally above the yield stress, i.e., if $F > 0$, in this case $\dot{\lambda}$ is iteratively adjusted to satisfy the conditions

$$\dot{\lambda} \geq 0, F \leq 0, \dot{\lambda}F = 0. \quad (11)$$

In addition to the mechanical equations we solve the energy equation to account for shear heating (viscous heating)

$$\rho c_p \left(\frac{\partial T}{\partial t} + v_i \frac{\partial T}{\partial x_i}\right) = \frac{\partial}{\partial x_i}\left(k\frac{\partial T}{\partial x_i}\right) + H_s, \quad (12)$$

$$H_s = \tilde{\sigma}_{ij}\left(\dot{\varepsilon}_{ij} - \dot{\varepsilon}_{ij}^{el}\right) = \tilde{\sigma}_{ij}\left(\dot{\varepsilon}_{ij} - \frac{1}{2G}\frac{D\tilde{\sigma}_{ij}}{Dt}\right), \quad (13)$$

where k is thermal conductivity. Insulating thermal boundary conditions are applied.

[12] Viscosity is defined here by

$$\mu_{eff} = \mu_0 \left(\frac{\dot{\varepsilon}_{II}}{\dot{\varepsilon}_0}\right)^{\frac{1}{n}-1}, \quad (14)$$

where $\dot{\varepsilon}_{II} = (0.5\dot{\varepsilon}_{ij}\,\dot{\varepsilon}_{ij})^{0.5}$ is the second invariant of the strain rate tensor, μ_0 the characteristic viscosity, n the power law coefficient and $\dot{\varepsilon}_0$ the characteristic strain rate (note that in most experimentally derived flow laws $\dot{\varepsilon}_0 = 1$). Equation (14) implies that a shear thinning viscous rheology is characterized by power law exponents greater than unity, as is conventional in the geodynamics and solid rock deformation literature; this formulation is the inverse of the oft adopted convention in magmatic rheology where $n < 1$ is indicative of shear thinning (Appendix A). Problems involving nonlinear viscous rheology are solved iteratively until the change of resulting velocities is less than 0.1%. The general viscosity description can be modified according to the crystal or melt phase when temperature changes are taken into account. The relevant laws are given below.

3.2. Melt Rheology

[13] In order to perform simulations that can be compared with laboratory experiments, we use an empirically (phenomenologically) derived viscosity model to predict viscosities of natural volatile-bearing silicate melts [*Giordano et al.*, 2008, available from www.eos.ubc.ca/~krussell]. This model depends on temperature and composition. For present purposes we assume the melt composition (2.88% H_2O, 77.2% SiO_2, 11.52% Al_2O_3, 3.78% Na_2O, 4.62% K_2O in weight percent) from the experiments of *Caricchi et al.* [2007] so that

$$\log_{10}(\mu^{gio}) = a + \frac{b}{T - c}, \quad (15)$$

where $a = -4.5$, $b = 11249$, and $c = 35.302$ are composition-dependent parameters, and T is the temperature in Kelvin. We generalize this expression to account for nonlinear viscous behavior of the melt as

$$\mu_{eff}^{melt} = f\mu^{gio}\left(\frac{\dot{\varepsilon}_{II}}{\dot{\varepsilon}_0}\right)^{\frac{1}{n}-1}. \quad (16)$$

If temperature is constant, we compute μ_{eff} with equation (14). The factor f is a viscosity multiplier, which allows us to increase the viscosity to levels at which it is possible to achieve the large stresses observed in laboratory experiments.

3.3. Numerical Method

[14] The equations described above (equations (3)–(16)) are solved using the finite element (FE) code MILAMIN_VEP (see e.g., *Kaus* [2010] for details). To obtain accurate solutions given the large viscosity contrasts in a melt-particle system, we use a Lagrangian mesh with P_2P_{-1} 7 node Crouzeix-Raviart triangular elements [*Cuvelier et al.*, 1986], with quadratic shape functions for velocity and linear, discontinuous shape functions for pressure. The body-fitting mesh (elements exactly follow the crystal-melt boundaries) is generated using

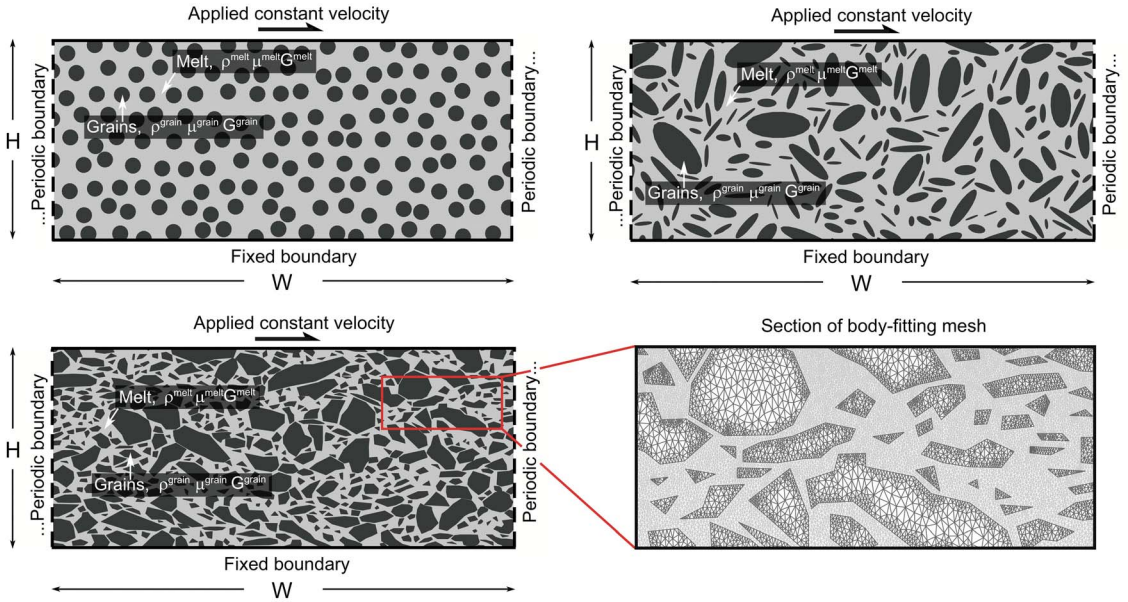

Figure 3. Model domain used for computations with randomly distributed spherical and elliptical particles and interstitial melt. In some cases, natural crystal shapes are used, which are digitized from laboratory experiments. Simple shear boundary conditions are applied. Numerical simulations are performed with body-fitting meshes (lower left).

TRIANGLE [*Shewshuk*, 1996]. If the elements become too distorted, remeshing is applied. Remeshing introduces errors, which are visible as small offsets in the computed stress-strain curves. The magnitude of the offsets is reduced if the number of elements in the simulation is increased, but the overall stress-strain curves remain similar, which suggests that the results obtained here are resolution independent. Typically 100′000–205′000 elements were used for a simulation.

[15] The Lagrangian FE method yields accurate results for our problem configuration [*Deubelbeiss and Kaus*, 2008] and has been successfully applied in an earlier study dealing with particle suspensions [*Deubelbeiss et al.*, 2010]. Tracers are employed to track material properties. Material properties are computed from the tracers by computing the dominant phase at each integration point, after which the integration point values are averaged over the element.

3.4. Model Setup

[16] We use a 2-D simple shear setup consisting of suspending particles and interstitial melt. The initial location of the particles is random. Simulations are performed for spherical and elliptical particles as well as for crystals with natural shapes (Figure 3). Physical parameters vary depending on different tests and are given in Table 1.

[17] Simple shear deformation is induced by applying a constant horizontal velocity at the top boundary (with zero vertical velocity), while the bottom boundary is fixed. To enable simulations with large strains we impose periodic lateral boundaries. Thermal boundary conditions are insulating, which implies that we compute the maximum shear heating effect.

[18] Stress-strain curves are computed for the numerical simulation by calculating the aggregate (bulk or also average) values of the stresses as follows: for each element an average value is derived by taking the mean of the values at the integration points and multiplied by the area of the element. The average of the total aggregate is then the sum of the element-wise averaged values divided by the sum of the area of each element. The aggregate viscosities are derived by the macroscopic stress-strain rate relationship that is the aggregate viscosity is

$$\mu^{agg} = \frac{\tilde{\sigma}^{agg}}{2\dot{\varepsilon}^{agg}}, \tag{17}$$

where $\tilde{\sigma}^{agg}$ and $\dot{\varepsilon}^{agg}$ are the deviatoric stresses and the strain rates averaged over the elements. The aggregate properties are determined every time step.

Table 1. Physical Parameters Used in the 2-D Numerical Experiments

Physical Parameter	Description	Value	Remark
W	Width of domain	1885 μm	[a]
H	Height of domain	700 μm	[a]
S	Grain size	50–100 μm	[a]
μ^{melt}	Initial viscosity of melt	3.3×10^{8}–2×10^{12} Pa s	[b]
$\mu^{crystal}$	Initial viscosity of crystal grains	$10^{6} \times \mu^{melt}$	
ρ^{melt}	Density of melt	2200 kg/m^3	
$\rho^{crystal}$	Density of crystal grain	2800 kg/m^3	
$\dot{\varepsilon}_{BG}$	Background strain rate	$5 \times 10^{-6} - 10^{-1}$ s^{-1}	[c]
G	Elastic shear modulus	$10^{9} - 10^{10}$ Pa	[d]
c_p	Heat capacity	1300 J/kg/K	
T_0	Initial temperature	600°C	
C	Cohesion (in plasticity simulations)	15–30 MPa	[c]

[a]Ten times larger for spherical and elliptical particles.
[b]Mostly 2.4×10^{9} Pa s. The use of larger viscosity values compared with laboratory experiments are justified by the smaller aggregate viscosities (and therefore stresses) that occur in 2-D compared to 3-D setups.
[c]Varied as indicated in the text.
[d]Varied in order to obtain similar viscoelastic relaxation times as in laboratory experiments.

For shear viscosities only shear components ($\tilde{\sigma}_{xy}^{agg}$, $\dot{\varepsilon}_{xy}^{agg}$) are used.

[19] For simplicity, shear aggregate viscosity (μ_{xy}^{agg}) is called aggregate viscosity μ throughout this paper (the aggregate viscosity is sometimes referred to as the apparent suspension viscosity in magma rheology literature). In numerical context, where it is clear, aggregate viscosity is only referred as viscosity, while the melt viscosity is defined explicitly as μ^{melt}.

4. Effective Aggregate Rheology in 2-D Numerical Simulations

[20] We perform a series of finite strain forward simulation in order to test the relative importance of finite strain effects (microstructural reordering of crystals), shear heating, power law melt rheology and plasticity on the aggregate rheology of melt-crystal suspensions. Systematic testing is for the case of spherically particles, and is augmented by simulations with elliptical and natural particle shapes. Two kinds of tests are performed: the strain rate is kept constant; or it is increased in a stepwise manner after reaching for each step a steady state stress. The first setup allows us additionally to investigate finite strain effects of the aggregate rheology with increasing strain, while the second is mainly used to investigate the dependence of aggregate rheology on strain rates and to compare numerical with experimental results.

4.1. Rheological Combinations

[21] We consider the following four rheological models: (1) model A, Newtonian melt rheology, which includes constant temperature and a linear viscous melt rheology (equation (14) with $n = 1$), (2) model B, non-Newtonian melt rheology including shear heating, which includes temperature-dependent viscosity according to *Giordano et al.* [2008] (equation (16)), with $n = 1$), (3) model C, non-Newtonian melt rheology including power law rheology, which includes nonlinear melt rheology with a power law coefficient $n > 1$, and (4) model D, non-Newtonian melt rheology including plasticity, which includes linear viscous melt rheology including plastic deformation of either crystal or melt phase for a given yield stress.

[22] The viscous component of the solid particle rheology is chosen so that the irreversible time-dependent deformation of the particles is insignificant. However, in simulations with plasticity, crystals fail plastically. Elasticity is employed in all numerical simulations to reproduce the stress-strain response observed in laboratory experiments [e.g., *Dingwell and Webb*, 1990; *Bagdassarov et al.*, 1994].

4.2. Results for Spherical Particles

4.2.1. Newtonian Viscous Rheology (Model A)

[23] In typical simulations (Figure 4) with Newtonian viscous melt rheology (model A) and spherical particles at lower strains the particles with little

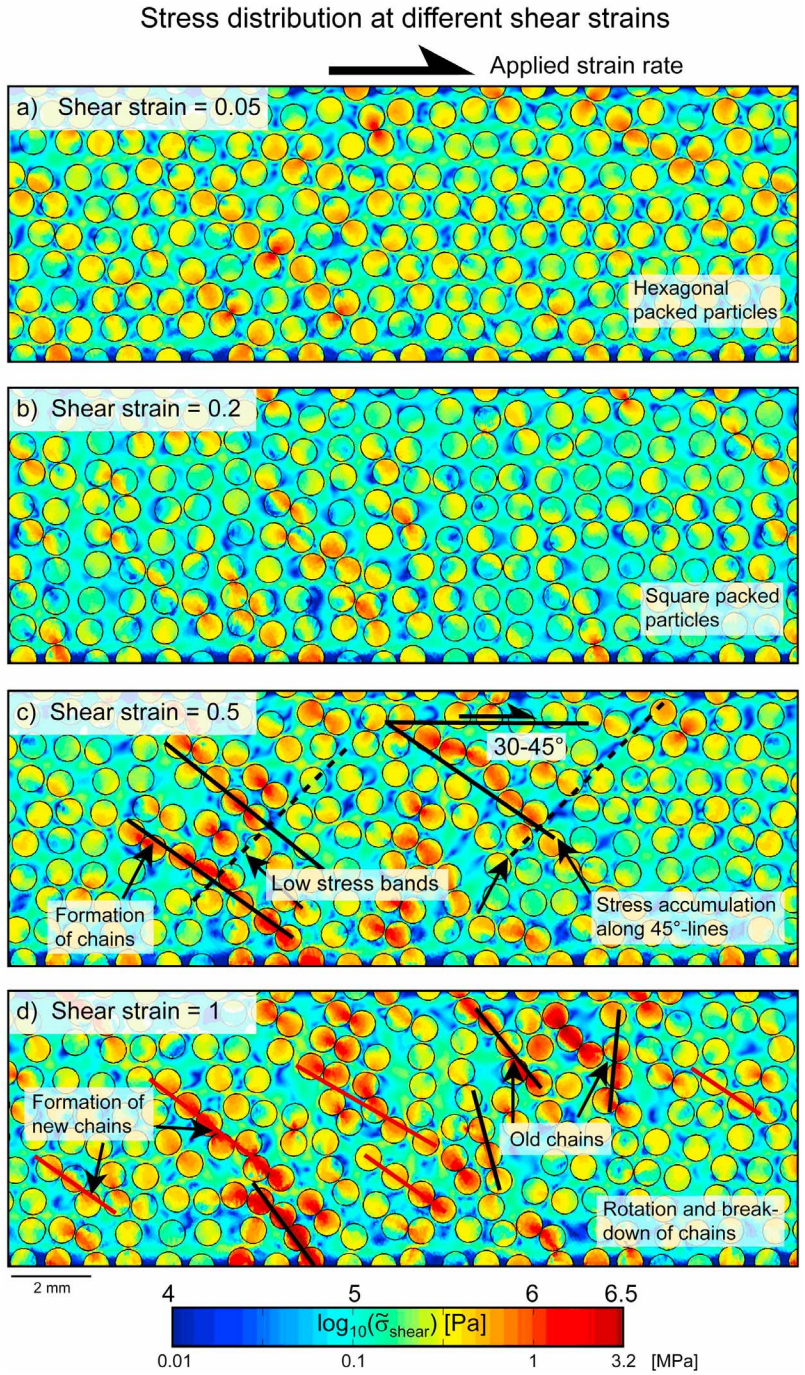

Figure 4. Stress distribution for different shear strains for a simulation with a solid fraction of $\phi_s = 0.5$ deformed with $\dot{\varepsilon} = 7 \times 10^{-5}$ s^{-1}. (a) Relatively homogeneously distributed stresses. (b) A square packed crystal network (which results in a minimum in the aggregate viscosity). (c) Crystals arrange in lines (30–45° to the applied strain rate). (d) Rotation of chains from 45° facing north-west to 45° facing north-east allows individual crystals to move, while simultaneously new chains are formed. At strains where stresses increase abruptly, crystals are arranged such that it is difficult to change the relative position and stresses accumulate, which causes an increase in aggregate viscosity.

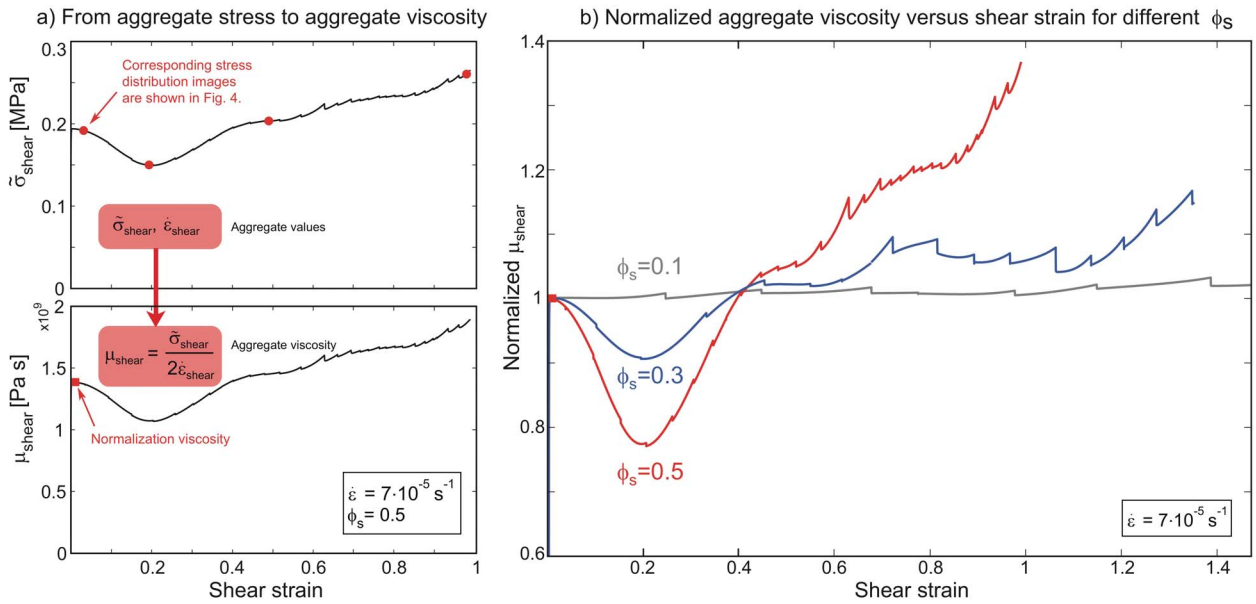

Figure 5. Simple shear simulation using Newtonian viscous rheology (model A). Simulations are performed at constant strain rate and have melt viscosity $\mu^{melt} = 3.3 \times 10^8$ Pa s and elastic shear module $G = 10^9$ Pa. (a) Aggregate stress and viscosity computed for whole sample versus strain for the simulation of Figure 4. (b) Normalized viscosities versus shear strain for different solid fractions. Strain weakening and strain hardening are related to a rearrangement of the particles inside the system (see also Figure 4 and text for details). The small abrupt offsets in the curves are due to remeshing. The minimum in viscosity around $\varepsilon = 0.2$ occurs at a stage when the particles are approximately cubically packed (Figure 4b).

interference but at larger strains the particles align at an angle of 30–45° related to the shear plane (chains), which coincides with the orientation of largest principle stress. At the same angle, inversely oriented (direction of lowest principal stress) low-stress bands develop. With increasing shear deformation the chains of aligned particles begin to rotate and break up (Figure 4d).

[24] The numerical simulations with spherical particles show an initial decrease of the aggregate viscosity (strain weakening) that is followed by an increase (strain hardening) at larger strains (Figure 5a). The initial drop in viscosity occurs when the particles move from a hexagonal packing into a square packing, which produces more horizontal melt channels (Figures 4a and 4b). The increase in viscosity coincides with the arrangement of particles in lines (Figure 4c). The accumulation of stress increases abruptly when particles are optimally oriented along lines (chains), such that it is difficult to change the relative position between the particles. The total amount of strain weakening and hardening depends on the solid fraction (Figure 5b) and is insignificant at small solid fractions. With increasing solid fraction mutual obstruction of the particles becomes more important so that more high-stress chains are formed. Our results are consistent with previous models of heterogeneously sized solid suspensions that reported similar force chains [*Morgan and Boettcher*, 1999].

[25] Simulations using strain rate stepping for the same set up show a nearly identical viscosity curve with strain weakening and hardening (Figure 6). This similarity indicates that the strain weakening and hardening that occurs up to is caused by a rearrangement of the crystals and not by an increase of the strain rate. The slightly smaller viscosities for $\dot{\varepsilon} = 3.5 \times 10^{-3}$ s^{-1} are explained by the breakdown of chains, that is a sudden increase to a higher strain rate breaks some of the chains. However, with increasing strain new chains are formed resulting in higher stresses and therefore viscosities increase as well, similar to the constant strain rate simulations. Additional simulations with strain rate stepping at different strains resulted in identical viscosity curves, further supporting the conjecture that the effect is caused by particle rearrangement.

[26] The maximum power law coefficient for a strain rate stepping test was $n = 1.29$. Simulations as a function of crystal size suggest that crystal size is not an important source of variability (Appendix B).

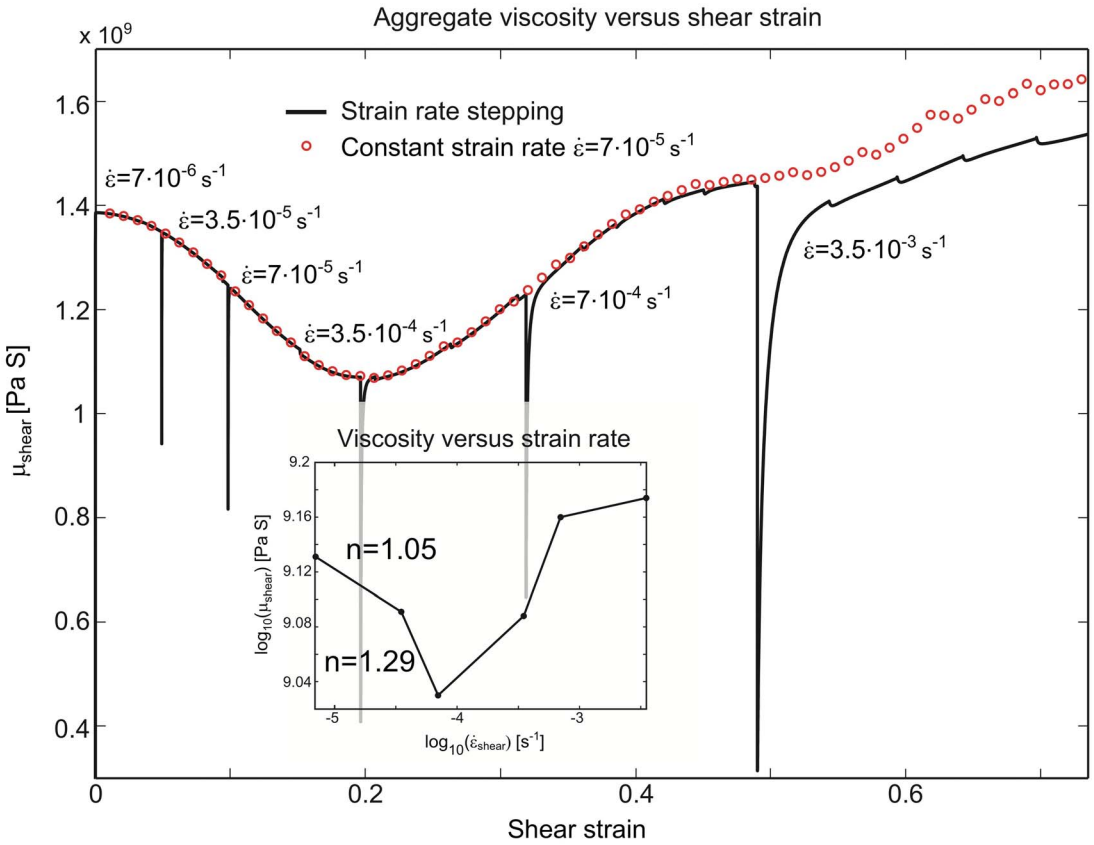

Figure 6. Viscosity versus strain for a simulation using constant strain rate (open circles) and one using strain rate stepping (solid line). Parameters are as in Figure 4. Inset shows viscosity versus strain rate extracted from the strain rate stepping simulation, where the viscosity at the end of one strain rate step was picked. The maximum power law coefficient is obtained in this simulation is $n = 1.29$.

4.2.2. Shear Heating (Model B)

[27] Simulations at different strain rates and different solid fractions were undertaken to test whether shear heating is the cause of nonlinear viscous magma rheology [e.g., *Hess et al.*, 2008; *Mueller et al.*, 2010]. To test whether shear heating has an effect on crystal-melt systems we perform simulations at different strain rates and different solid fractions.

[28] Because viscous rheologies are thermally activated shear heating causes a reduction in viscosity (Figure 7) that is manifest as shear thinning if the temperature dependence of the rheology is explicitly taken into account. Shear heating increases for increasing strain rates. In our simulations, the apparent power law coefficient of a linear viscous material reaches a maximum of $n = 3.15$ (Figure 7b).

[29] Shear heating increases with solid fraction probably because (1) the average stress in the aggregate increases with solid fraction, and (2) at high solid fractions, local strain rates are considerably greater than the applied background strain rate [*Deubelbeiss et al.*, 2010]. Similar to simulations in which strain rate is varied, viscosities decrease with increasing strain (Figure 7c). The amount of viscosity reduction increases with increasing solid fraction (Figure 7d). These effects are not investigated in detail because the effect of solid fraction on aggregate viscosities have been addressed in a number of experimental or theoretical studies [*Roscoe*, 1952; *Pinkerton and Stevenson*, 1992; *Lejeune and Richet*, 1995; *Costa*, 2005; *Caricchi et al.*, 2007; *Cordonnier et al.*, 2009; *Costa et al.*, 2009; *Petford*, 2009; *Deubelbeiss et al.*, 2010].

4.2.3. Shear Heating Analysis With a 0-D Model

[30] In order to determine how accurately our 0-D model predicts the adiabatic temperature increase of real models, we compared 2-D numerical results with predictions from our 0-D model. Therefore, we

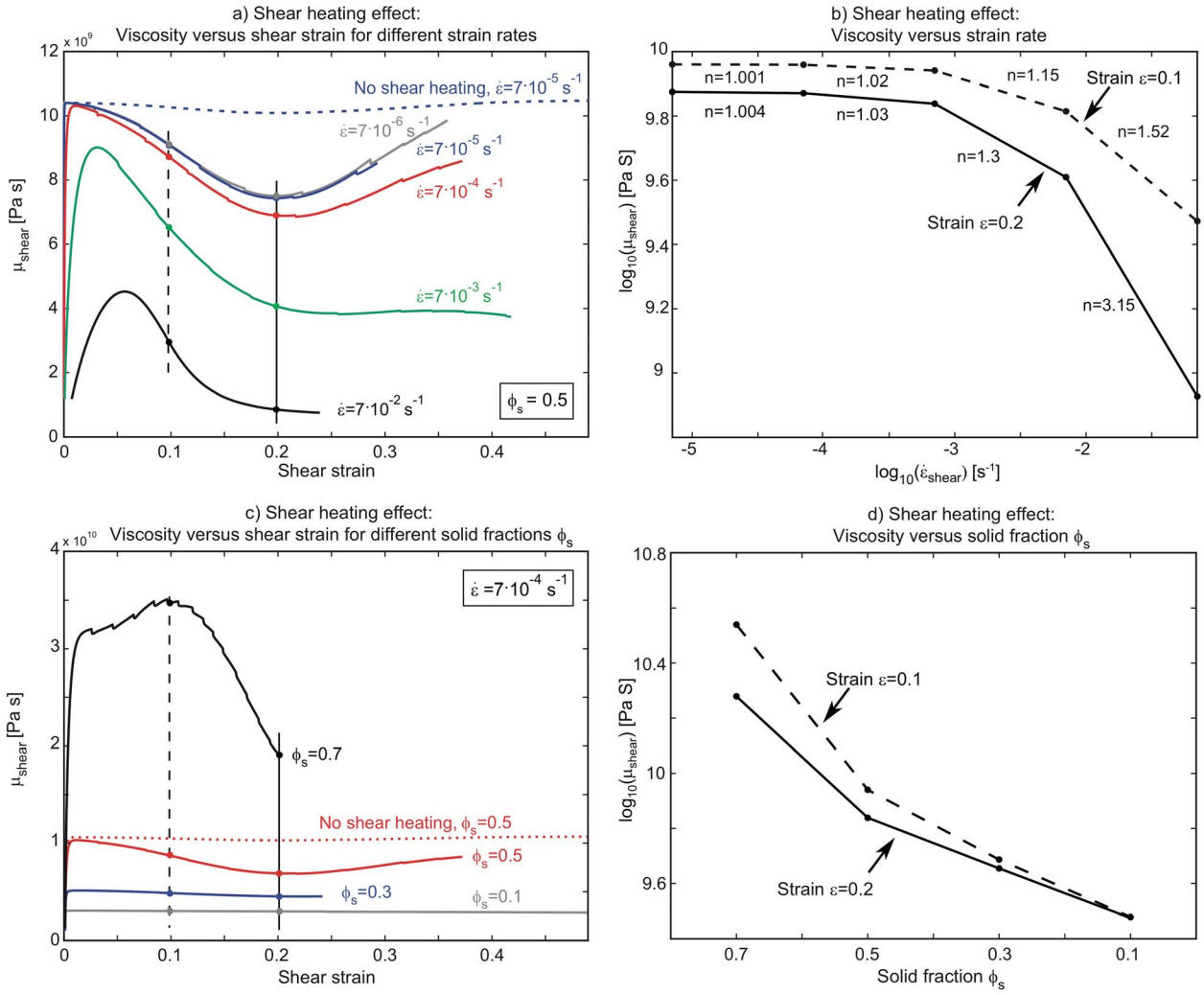

Figure 7. Shear heating tests (model B) with initial melt viscosity $\mu^{melt} = 2.4 \times 10^9$ and elastic shear module $G = 10^9$ Pa s. (a) Viscosity versus shear strain for different strain rates and a constant solid fraction $\phi_s = 0.5$. For comparison, a simulation without shear heating is also shown. (b) Viscosity versus strain rate curves indicate an increasing power law coefficient with increasing strain rate with a maximum $n = 3.15$. (c) Viscosity versus shear strain for different solid fractions and a constant strain rate $\dot{\varepsilon} = 7 \times 10^{-4}$ s^{-1}. (d) Viscosity decreases with decreasing solid fraction and increasing strain.

used numerically computed stress-strain curves as input for the 0-D inversion algorithm. The 0-D model agrees well with the numerically calculated temperature increase for changing strain rates and changing solid fractions. Additionally, the 0-D model predictions are in good agreement with *Hess et al.* [2008]. Temperature increases are only large for strain rates above 10^{-2} s^{-1} (Table 2).

[31] Using the 0-D model to extract the heat production from experimentally derived stress-strain curves, we obtain an increase of no more than $\Delta T = 2.8$°C for parameters comparable with experiments of [*Caricchi et al.*, 2007] ($\phi_s = 0.5$, $\dot{\varepsilon} = 10^{-4}$ s^{-1}, $\varepsilon = 0.2$, $G = 10^{10}$ Pa, initial temperature of 600°C and an aggregate viscosity of 2×10^{11} Pa s, which is high in order to reach stresses of ≈40 MPa (note that the high viscosity values are justified by the smaller aggregate viscosities that occur in 2-D compared to 3-D simulations).

4.2.4. Power Law Melt Rheology (Model C)

[32] It is not known if the interstitial melt of a suspension exhibits non-Newtonian viscous behavior. It has been shown that single-phase silicate melt undergoes a transition from Newtonian to a non-Newtonian rheology at approximately 3 orders of magnitude slower strain rates than that predicted by Maxwell relaxation [*Webb and Dingwell*, 1990a,

Table 2. Temperature Increase Computed With the 0-D Model at Strain[a]

Physical Parameter	Description	Values for $\phi = 0.5$			Values for $\phi = 0.7$
ϕ	Solid fraction	0.5	0.5	0.5	0.7
	Strain rate	7×10^{-2} s^{-1}	7×10^{-3} s^{-1}	7×10^{-4} s^{-1}	7×10^{-4} s^{-1}
ΔT	Temperature increase predicted with 0-D model	65°C	9.5°C	0.98°C	3.2°C
ΔT	Temperature increase measured in 2-D simulations	44°C	9.2°C	1.2°C	3.5°C

[a]Compared with observed values in 2-D numerical simulations that are the parameters of Figure 7 with initial temperature of $T_0 = 600$°C.

1990b] For the parameters employed in our numerical simulations the Maxwell relaxation time τ_{relax} and the relaxation strain rate $\dot{\gamma}_{relax}$ (according to equation (1) in the work of *Webb and Dingwell* [1990a]) is

$$\tau_{relax} = \frac{\mu_s}{G_\infty} = \frac{2.4 \times 10^9 \text{Pas}}{10^{10} \text{Pa}} = 0.24 \text{ s} \quad (18)$$

$$\dot{\gamma}_{relax} = \tau_{relax}^{-1} = 4.2 \text{ s}^{-1}, \quad (19)$$

where μ_s is the zero frequency Newtonian shear viscosity which we take to be the melt viscosity and G_∞ is the infinite frequency elastic shear modulus of the melt which is here the elastic shear modulus of the numerical simulation. Using these equations, we can estimate the resulting strain rate at which the rheology might change from Newtonian to non-Newtonian to be ~4.2×10^{-3} s^{-1}. With increasing viscosity the relaxation strain rate decreases and thus the transition takes place at smaller strain rates (relations between viscosity and solid fraction are given in the work by *Deubelbeiss et al.* [2010]). Because strain rates are locally significantly larger between crystals than the bulk strain rate of the aggregate [*Deubelbeiss et al.*, 2010], it may thus be possible to trigger a transition in rheology on a local scale. For this reason, we performed a few numerical simulations to study what the influence of power law melt rheology on crystal-bearing melts is (model C).

[33] The resulting aggregate power law coefficients reproduce exactly the original input power law coefficient of the melt [*Deubelbeiss*, 2010]. In our previous work, we already demonstrated that the power law coefficient of the solid particles does not influence the overall behavior of the aggregate, predominantly because the particles effectively behave rigid [*Deubelbeiss et al.*, 2010]. Thus, in order to explain aggregate power law coefficients of up to 13, one needs a melt rheology with the same n value.

4.2.5. Plasticity (Model D)

[34] Experiments of *Caricchi et al.* [2007] show a reduction of grain size, most probably due to brittle failure of individual crystals, which might additionally affect the aggregate rheology. To test the influence of plastic failure on crystal-melt systems, we perform simulations with a plastic rheology for the fluid and solid phase (model D) and a yield stress of 15 MPa, which is justified as the fluid pressure is large in the simulations and because we underestimate viscosities (and hence stresses) in 2-D compared to 3-D simulations.

[35] As the solid particles typically have the largest differential stresses (Figure 4), they are the location at which the first plastic failure occurs. With increasing strain rate the aggregate viscosities decrease (Figure 8a). The resulting viscosity versus strain rate curve (Figure 8b) shows an increase of power law coefficients with increasing strain rate starting with $n = 1.16$ and reaching values of up to $n \approx 50$. Numerical results using comparable parameters to experiments of *Caricchi et al.* [2007] with resulting aggregate stresses of about 130 MPa, still reach power law coefficients of $n \approx 5$.

4.3. Results for Elliptical Particles

[36] Crystal aspect ratio is an additional parameter that has a potential influence on aggregate rheology. To study this, we performed simulations with randomly distributed elliptical particles of variable aspect ratio and size for a Newtonian viscous melt rheology (model A). At small solid fraction, the simulation with elliptical particles has a slightly more time-dependent behavior than the simulation with spheres (Figure 9) for the same solid fraction. The fluctuations in viscosity are correlated with the rotation of particles and a minimum viscosity is obtained once particles are optimally aligned with the flow direction. The significant drop of viscosity at $\varepsilon = 0.2$ as observed in spherical particle simula-

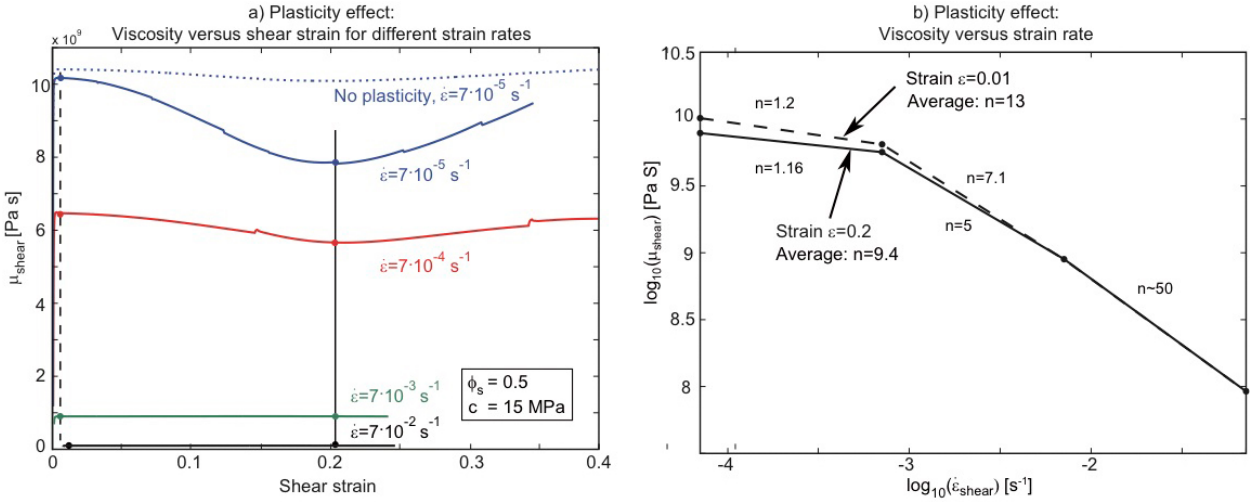

Figure 8. Effect of plastic failure (model D) for simulations with $\mu^{melt} = 2.4 \times 10^9$ and $G = 10^{10}$ Pa. (a) Viscosity versus shear strain for different strain rates. For comparison we also show a simulation without plasticity. Plasticity results in significantly smaller values of aggregate viscosity. (b) Viscosity versus strain rate curves indicate an increasing power law coefficient with increasing strain rate up to maximum $n \sim 50$ measured at strain $\varepsilon = 0.2$. This value occurs for a very large applied strain rate of $\dot{\varepsilon} = 7 \times 10^{-2}$ s^{-1}, which results in aggregate stresses of more than 600 MPa and plastic failure of both melt and crystals. However, power law coefficients of up to $n = 5$ are obtained for more reasonable values of strain rate ($\dot{\varepsilon} = 7 \times 10^{-3}$).

tions does not occur due to more heterogeneously distributed particles with different size and different aspect ratios.

[37] We performed a strain rate stepping test for a simulation with a larger solid fraction. Compared to the simulation with smaller solid fraction, particles rotate slower and are in some cases bent, which is likely due to mutual obstruction of the particles (Figure 10). The power law coefficient determined from this experiment is rather small (n = 1.02), which is also visible in the viscosity plot, which shows only a minor decrease with increasing strain.

4.4. Naturally Shaped Crystals

4.4.1. Results

[38] So far, all results were obtained for a synthetic setup with elliptical or spherical particles. As real grains rarely have this shape, we also performed a variety of simulations with more realistic particle

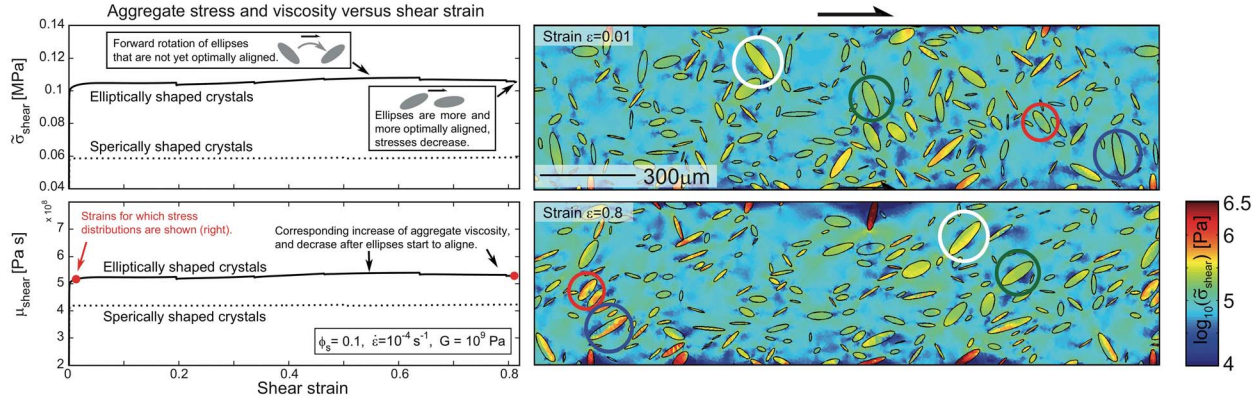

Figure 9. Numerical simulation using elliptically shaped crystals with Newtonian viscous rheology (model A, with $\phi_s = 0.1$ $\mu^{melt} = 3.3 \times 10^8$ Pa s, $\dot{\varepsilon} = 10^{-4}$ s^{-1}). A simulation using spherically shaped crystals with the same solid fraction is shown for comparison. Stresses in this simulation are smaller because the applied strain rate is slightly smaller ($\dot{\varepsilon} = 7 \times 10^{-5}$ s^{-1}). Note that the viscosity with spherical particles reaches a steady state, whereas the one with elliptical particles oscillates, which is caused by rotating particles (as indicated on the right by colored circles).

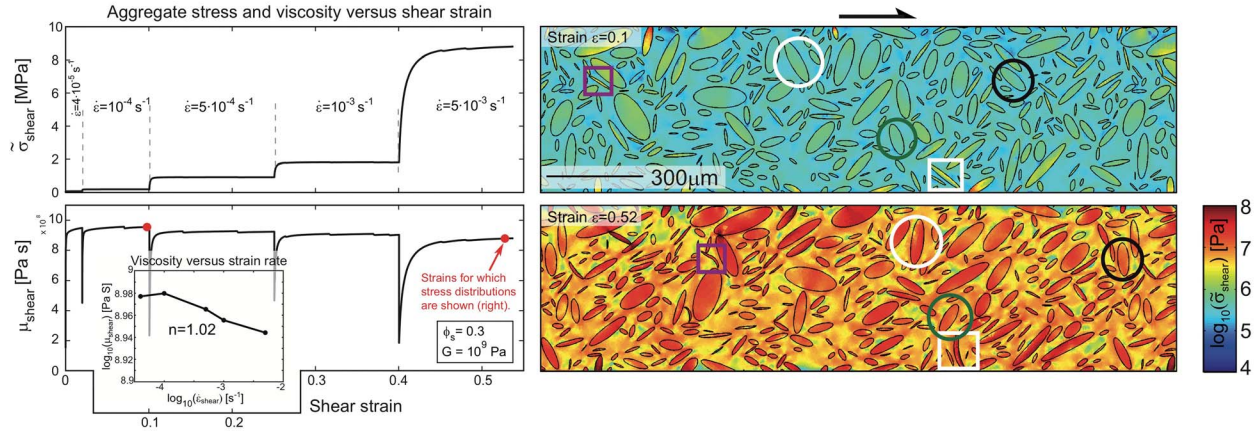

Figure 10. Numerical simulation using elliptically shaped crystals with larger solid fraction (model A with $\phi_s = 0.3$). The power law coefficient determined from this experiment is $n = 1.02$. Note that some particles are bend during ongoing deformation (colored circles).

shapes obtained from a digitized backscattered electron image that was taken at a strain of $\varepsilon = 0.025$ (note that $\gamma = 2/\varepsilon = 0.05$, γ is usually used to define strain in laboratory experiments) of a laboratory experiments (Figure 11a). As our experiments are two-dimensional, they underestimate stresses compared to 3-D settings [*Deubelbeiss et al.*, 2010]. In order to obtain comparable average stresses as in laboratory experiments (and therefore simulate brittle failure in a more realistic manner), we increased the melt viscosity.

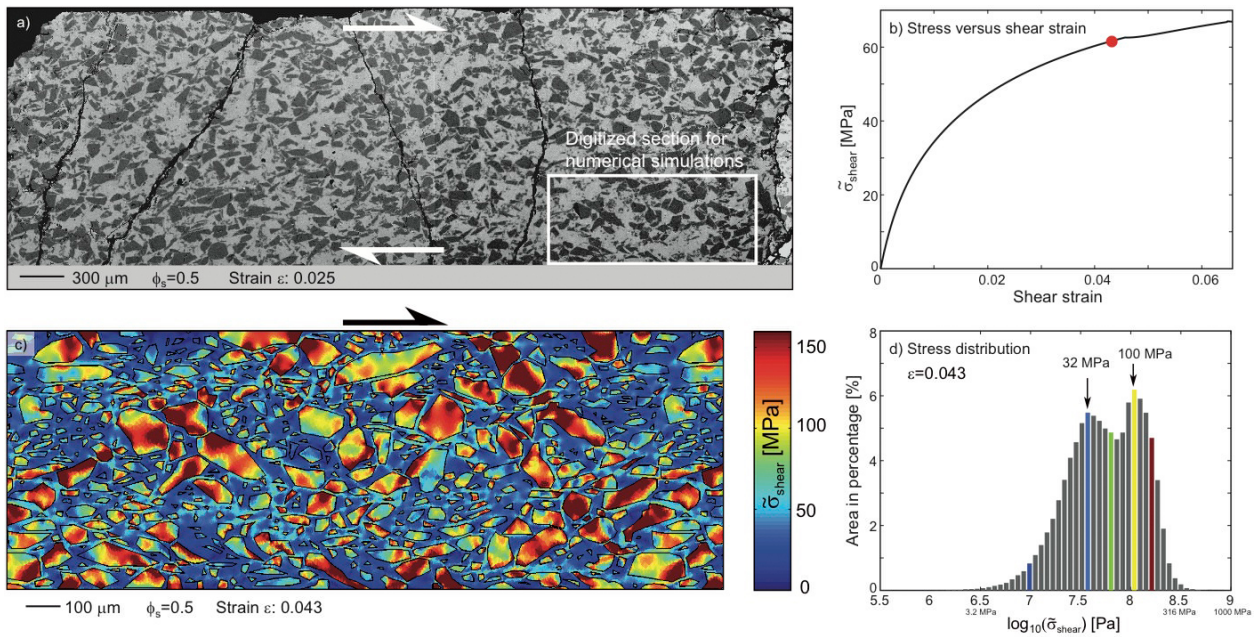

Figure 11. (a) Back scattered electron image of a laboratory experiment of *Caricchi et al.* [2007] with solid fraction $\phi_s = 0.5$ after a strain of 0.025. (b) Stress-strain curve of the numerical experiment, in which we employed $\mu^{melt} = 2 \times 10^{12}$ Pa s, $G = 1.5 \times 10^9$ Pa, and $\dot{\varepsilon} = 4 \times 10^{-6}$ s^{-1}. (c) Spatial stress distribution of the numerical simulation after a strain of 0.043 (indicated by a red dot in Figure 11b). High stresses occur at 45° angles to the flow direction. Also note the high-stress band that develops within the melt at very low angle. These bands are present in the digitized image. (d) A histogram of stress versus area shows that two peaks occur: one at 32 MPa (corresponding to the stresses within the melt) and another one around 100 MPa, which corresponds to stresses within the crystal. The maximum stress is ≈1000 MPa, even though the average sample stress is only around 60 MPa (see Figure 11b).

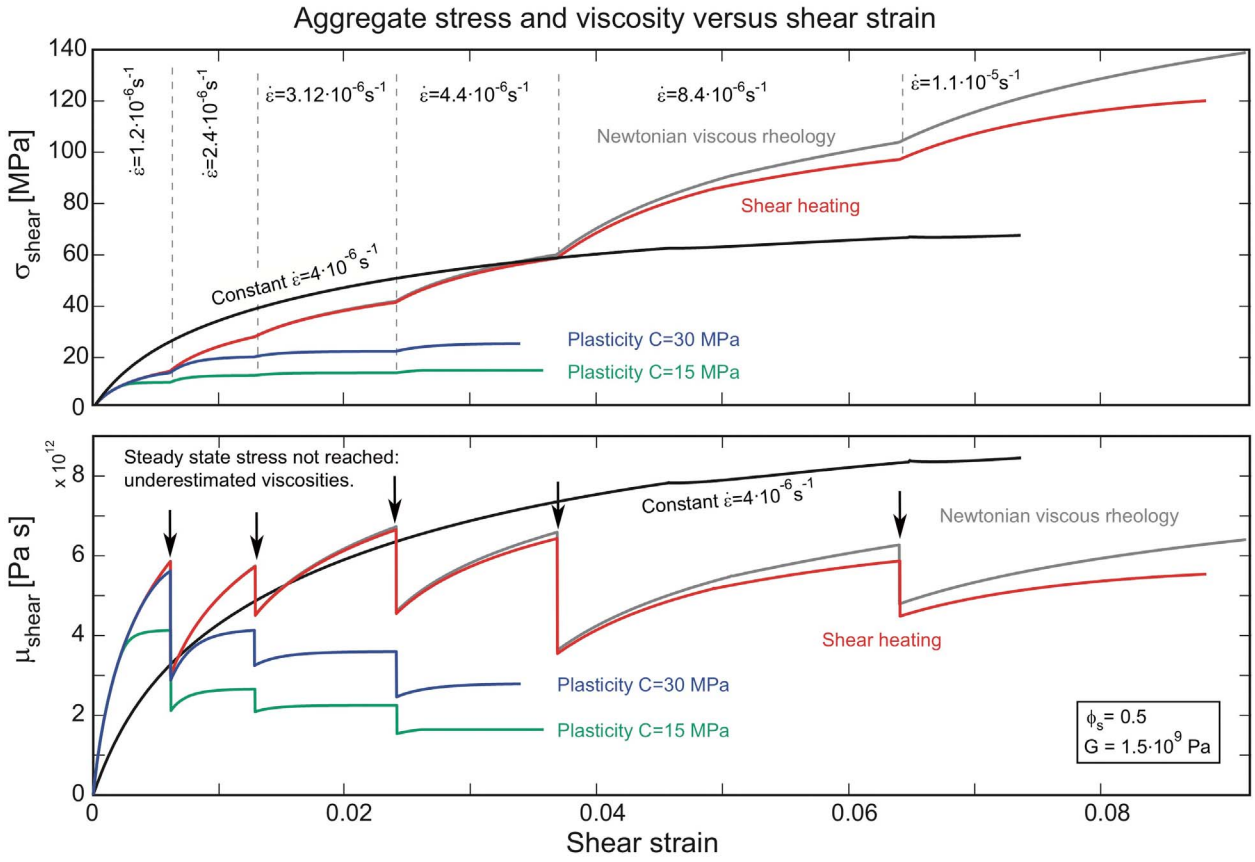

Figure 12. Stress/viscosity versus strain for various simulations with crystals, in which the effect of shear heating and plasticity was tested and compared to a purely Newtonian simulation (model A). Parameters are the same as in Figure 11. Shear heating results in a small reduction of viscosity compared to a purely Newtonian simulation. The effect of plasticity (brittle failure of crystals) has a larger effect.

[39] Results for a purely Newtonian rheology (model A) show that high-stress bands occur in crystals at roughly 45° to the shear direction. Within the melt, the maximum stresses occur along low-angle bands, in which more small crystals are present (Figure 11c). The quantitative analysis of the stress distribution of this snap shot shows that two peaks occur: one is related to the stress distribution within the melt and one to the stress within crystals (Figure 11d). The maximum stresses occur within crystals and can be more than 15 times larger than the sample-averaged stresses. Combined with a relatively large fluid (melt) pressure, it is likely that such large stresses would induce brittle failure of crystals.

4.4.2. Influence of Finite Strain, Shear Heating, and Plasticity

[40] In order to study the effect of finite strain on natural crystal-melt systems, we performed a simulation at constant strain rate. The results did not show a strain weakening effect such as the one that was observed in the corresponding simulation with spherical particles (Figure 5). We attribute this to the fact that the crystal simulation has a more heterogeneous crystal shape and size distribution. Moreover, the starting geometry was taken from a laboratory experiment that was already slightly deformed.

[41] Next, we analyze the effect of shear heating and plasticity by performing strain rate stepping tests. Results show that the inclusion of shear heating results in only a minor drop in viscosity compared to a simulation without shear heating (Figure 12). Stresses obtained in the numerical simulation are comparable to those measured in the laboratory experiments, suggesting that the amount of shear heating is comparable as well. Note that the shear heating simulation shows a minor reduction in maximum viscosity versus strain. This should not be interpreted as a true shear thinning effect, as the simulations with larger strain rate did not yet

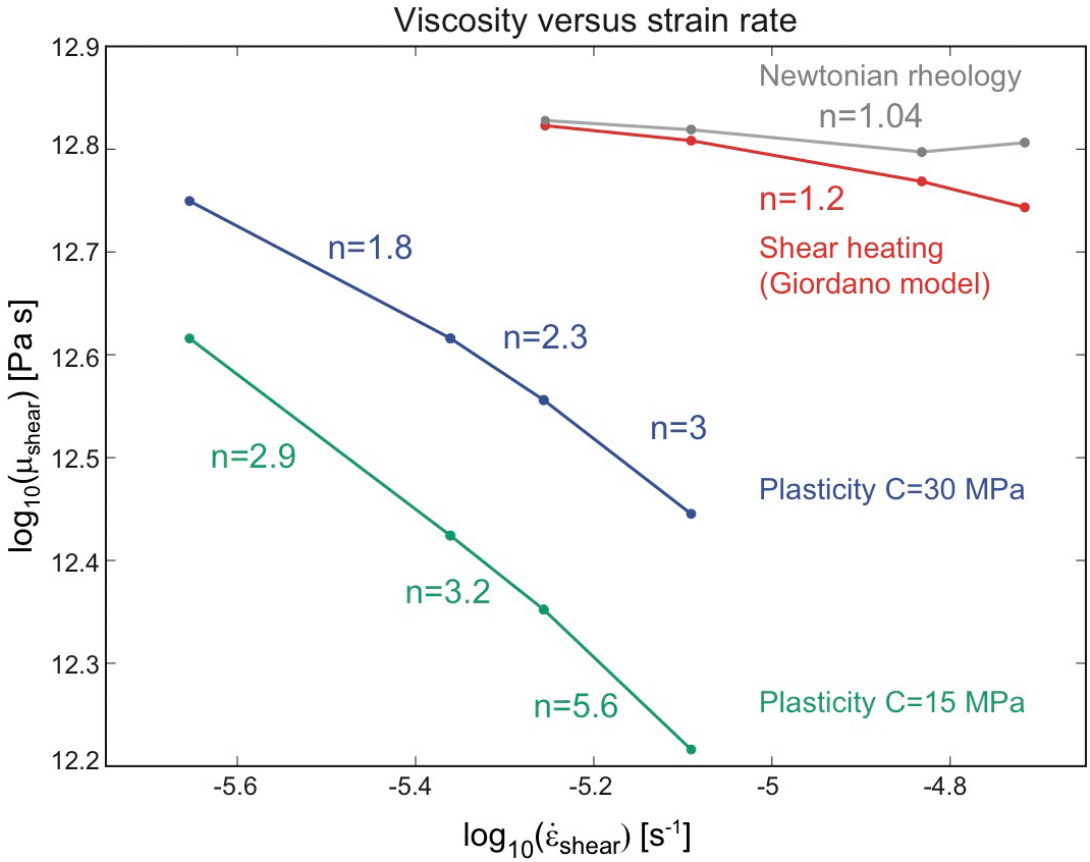

Figure 13. Power law coefficients computed from the numerical simulations shown in Figure 12.

reach a steady state stress before the strain rate was increased. Our 0-D algorithm is capable of extracting the true viscosity in these cases.

[42] Plasticity, on the other hand, does result in a significant reduction of viscosity (Figure 12), particularly in locations where the stresses are higher than the given yield stress. For very large strain rates, stresses within the melt exceed the yield stress and fail in a brittle manner as well. In these simulations a true shear thinning effect occurs, which is larger for smaller values of cohesion.

[43] The power law coefficients measured for these experiments, show that the effect of shear heating is rather minor and results in n = 1.2 compared to n = 1.04 for a nonshear heating experiment. Plasticity, on the other hand, results in lager coefficients of n = 3 and n = 5.6 (Figure 13).

5. Discussion

[44] We investigated potential causes for the non-Newtonian viscous rheology of crystal-bearing magmas. Often cited explanations for the non-Newtonian viscous rheology are shear heating [e.g., *Lavallée et al.*, 2007, 2008; *Mueller et al.*, 2010], reordering of crystals [*Völtz et al.*, 2002; *Caricchi et al.*, 2007; *Cordonnier et al.*, 2009] and fracturing of crystals [e.g., *Lavallée et al.*, 2008]. We used numerical simulations to explore the relative importance of shear heating, power law melt rheology, finite strain effects (reordering) and plastic failure of individual crystals on the aggregate rheology of crystal-bearing magmas using spherically, elliptically and naturally shaped crystals. Here, we will discuss our results in the context of previous laboratory experiments.

5.1. Shear Heating

[45] Our numerical simulations with spherical particles showed that large strain rates are required to generate significant temperature increases. For strain rates closer to the ones employed in laboratory experiments we obtained temperature increases of only a few degrees. The resulting power law coefficient obtained in our simulations was n = 1.3,

which is far below the values observed in laboratory experiments (see Figure 2). Simulations using crystals with parameters adjusted to reach stresses similar to those of laboratory experiments (≈60 MPa) result in a temperature increase of ≈4°C at strains comparable to those of laboratory experiments. The resulting power law coefficient was only about $n = 1.2$.

[46] A comparison of the 2-D simulations with a 0-D model shows that the 0-D model does a good job in predicting the to-be-expected increase in temperature due to shear heating. This means that the laboratory experiments of *Caricchi et al.* [2007] should not have had more than several degrees of temperature increase.

[47] Our simulations should be considered as an upper bound, as we employed adiabatic temperature boundary conditions (which means that all thermal energy generated in the sample remains there). The boundaries in a laboratory experiment are probably closer to isothermal. In this case, thermal energy can escape the system. For typical sample sizes of a few millimeters and a thermal diffusivity of $\approx 10^{-6}$ m^2/s, the characteristic diffusion timescale is around 1 s. Since typical experiments last a few hours, thermal diffusion will almost certainly have equilibrated the sample temperature.

[48] The amount of shear heating could locally be much larger if crystals are forcefully 'jammed' together, as it might occur at large solid fractions. In this case a local, sharp, increase of temperature could occur, but in order for this to have an effect on the bulk rheology, crystals should realign faster than the thermal diffusion timescale.

5.2. Finite Strain Effects

[49] Reordering of spherical particles result in a strain-dependent aggregate viscosity due to reordering of particles. The maximum effect is obtained in simulations with nearly equal particle size, and the effect is larger for spherical particles ($n = 1.3$) then for elliptical particles of variable size ($n = 1.02$). In the two latter cases, the crystals are strongly heterogeneously distributed both in size, shape and aspect ratio. In both cases, the effective viscosity oscillates with increasing strain and both shear thinning and shear thickening is observed. Physically the effect seems to be related the optimal packing configuration (for spherical particles) as well as due to a rotation of elliptical particles in the flow direction (which lowers the viscosity). The larger the solid fraction, the more difficult it is for elliptical particles to rotate and the effect is thus less pronounced. An oscillating behavior of viscosity versus strain is also observed in analog experiments [*Mueller et al.*, 2010].

[50] Our simulations with crystals do not have such finite strain effects. Most likely this is because the digitized image was taken from the end of a laboratory experiment, at a stage when some of the crystals seem to have already broken into smaller crystals and high aspect ratio crystals are aligned in the direction of applied shear stress. They are thus probably already in a close-to-optimal arrangement and increasing strain is not further changing the viscosity significantly. It is very likely that a preferred arrangement of the crystals occurs during preparation of the sample, while it is possible to produce synthetic numerical models with mathematically random distribution, which was the case for spherical and elliptical particles.

[51] It is important to note that in all cases we observe a clear finite strain effect of the viscosity. If a strain rate stepping test is performed during an oscillating cycle, this finite strain effect might indeed give the impression that the material has a strain rate-dependent rheology (rather than a strain-dependent rheology). Yet, the obtained power law coefficients are rather small (maximum $n = 1.3$). Moreover, it is quite straightforward to test this in laboratory experiments, by performing experiments up to much larger strains. *Caricchi et al.* [2007] performed such tests and found no evidence for a strain-dependent weakening of the rheology. On the basis of our experiments, it thus seems unlikely that the large power law coefficients observed in some experiments are caused by finite strain or crystal reordering alone.

5.3. Power Law Melt Rheology

[52] Laboratory experimentalists typically use aggregate strain rates to estimate whether the melt can be expected to exhibit non-Newtonian viscous behavior or not [*Caricchi et al.*, 2007]. The bulk strain rate is then adjusted to assure that the melt is in the linear regime. The fallacy of this logic is that in a rigid particle suspension, strain is localized within the melt and therefore local strain rates within the melt may be orders of magnitude greater than the bulk strain rate [*Deubelbeiss*, 2010]. Thus, non-Newtonian melt behavior cannot be precluded a priori on the basis of bulk strain rates. For this reason, we performed simulations in which the melt has a power law rheology. Results show that the non-Newtonian response of the aggregate system is

characterized by the same power law coefficient as the one of the melt, meaning that a resulting aggregate power law coefficient of $n = 13$ requires a power law coefficient of $n = 13$ for the melt as well.

[53] Experiments performed on pure silicate melts indicate that the melt has a power law rheology if a critical strain rate is exceeded before it fails in a brittle manner [*Webb and Dingwell*, 1990a, 1990b]. We estimated power law coefficients from published viscosity-strain rate plots and found that there is a large variability which ranges from $n \approx 2$ [*Webb and Dingwell*, 1990a, Figure 4, Crater lake andesite] up to $n \approx 7.5$ [*Webb and Dingwell*, 1990a, Figure 3] or $n \approx 5$ [*Webb and Dingwell*, 1990a, Figure 4, nephelinite].

[54] However, since high strain rates only occur locally, the melt will only be non-Newtonian in certain locations. The overall effect of this on the aggregate rheology will thus be smaller than the power law coefficients of a pure non-Newtonian melt. Generally, it is thus plausible that a change to non-Newtonian rheology with moderate power law coefficients ($2 < n < 5$) is due to locally enhanced strain rates. Yet, it is unlikely that aggregate power law coefficients of $n = 13$ can be explained by this effect alone.

5.4. Plasticity

[55] Our simulations have shown that the maximum obtainable stresses are significantly larger than the aggregate stresses, particularly, if the crystal fraction increases. This, combined with high fluid pressures, makes it likely that crystals fail in a brittle (plastic) manner. Experiments of *Caricchi et al.* [2007] show a reduction of grain size, possibly due to cracking of individual crystals. In experiments on natural crystal-melt systems it has been demonstrated that at high applied stresses (>10 MPa), cracking of large phenocrystals and an alignment of the fragments produces flow bands, which ease the flow of a suspension and lower the viscosity [*Lavallée et al.*, 2007; *Lavallée et al.*, 2008; *Cordonnier et al.*, 2009]. For plausible geological parameters we showed that we can reach power law coefficients of up to $n = 50$ in simulations with spherical particles. This value might appear surprising at first, as it is significantly larger than typical laboratory-derived power law exponents. Yet, a perfectly plastic material theoretically has a power law exponent of $n = \infty$, which is thus consistent with our numerical experiments (in which only part of the sample deforms in a plastic manner).

[56] Numerical simulations using crystals with parameters adjusted to reach similar stresses as in laboratory experiments, reach power law coefficients of up to $n = 5.6$ despite the fact that the initial geometry already had a strong reduction in crystal size in some parts of the sample. Generally, stresses inside a system using natural crystals are larger, due to strongly angled crystals. This favors a potential failure of crystals inside crystal-melt systems. Plasticity, therefore, is the most plausible explanation for the high power law coefficients, of up to $n = 13.5$, observed in laboratory experiments of *Caricchi et al.* [2007].

[57] In our simulations, plastic failure does not result in a physical breaking of the crystals (mainly because of technical limitations). Yet, the general behavior of the aggregate viscosity (decreasing viscosity due to local decrease of stress) is similar. In laboratory experiments stresses accumulate inside crystals, thereby producing localized microshear zones, which allow crystals to break. This reduces the aggregate viscosity, whereas in numerical simulations this is achieved by a local lowering of the viscosity.

[58] In some numerical simulations the melt also exceeds the yield stress and fails in a plastic manner, which affects the aggregate viscosity. Magma fracturing is an effect that is plausible to occur and was experimentally tested for vesicular magma by decompression [*Webb and Dingwell*, 1990a; *Kameda et al.*, 2008]. The onset of fracturing depends on the yield stress and expansion time scale, which is comparable to the yield stress in our models and the strain rate at which our aggregate deforms. The relevant criteria in relation to our simulations is given by

$$\frac{\mu^{melt}\dot{\varepsilon}}{G} > 1. \tag{20}$$

For the parameters of our simulation ($\mu_{melt} = 2 \times 10^{12}$ Pa s, $G = 1.5 \times 10^{9}$ Pa), we thus need a strain rate of at least $\dot{\varepsilon} = 5 \times 10^{-4}$ s^{-1}. For viscosities normally used in laboratory experiments the strain rate at which failure occurs is larger, e.g., for $\mu_{melt} = 2 \times 10^{9}$ Pa s, it requires a strain rate of 5×10^{-1} s^{-1}. These parameters are in a realistic range and it is thus possible that plastic failure of the melt occurs in laboratory experiments.

5.5. Numerical Simulations and Future Laboratory Experiments

[59] Our numerical simulations give important indications on the dynamics of deformation of par-

ticle suspensions. Yet, there are some discrepancies between numerical models and laboratory experiments. The comparison of the results obtained by numerical simulations and laboratory experiments may help improving numerical codes and drive the future experimental effort. The numerical simulations highlight strain-related effects that have not been described in laboratory experiments performed on particle-bearing silicate melts.

[60] A number of reasons could account for such differences. The precision of experimental measurements is limited in comparison to the numerical simulations and consequently the stress oscillations recorded during the numerical simulation are unlikely to be visible in laboratory experiments. The accuracy of the load cell in the Paterson-type apparatus used during simple shear experiments by is ≈1 Nm, which translates in uncertainties of a shear stress of about 1 MPa [*Paterson and Olgaard*, 2000]. Figure 5 shows that the stress oscillations are about an order of magnitude smaller than the sensitivity of the load cell used in the experiments. Additionally, the laboratory experiments were performed to a total strain that was relatively small with respect to numerical simulations. Experiments performed to higher total strain could help characterizing more accurately the effect of strain on the rheology of particle suspensions (see e.g., *Champallier et al.* [2008] for a few examples on experiments in similar systems that were performed up to gamma = 21, yet apparently without a major effect of strain weakening).

[61] In numerical simulations there is always viscous fluid present around the particles. In laboratory experiments due to 3-D effects, it is possible that some particles are in direct contact, particularly once a critical solid fraction is exceeded [*Saar et al.*, 2001]. This could make particle clusters that form during deformation more stable with increasing strain. A similar effect is observed in numerical simulations with spherical particles in which chains remain stable with increasing strain. Particles in contact (clusters) thus might have an effect on the effective aggregate rheology with increasing strain. One way to test this is to use 3-D numerical simulations and perform a detailed 3-D analysis of deformed laboratory samples.

[62] The numerical models highlighted the importance of crystal fracturing on the power law coefficient of laboratory experiments. Similar nonlinearities will occur if the melt fractures. The local stresses and strain rates measured during the experiments between crystals are sufficiently large to induce fracturing of the melt phase and this would have profound implications for the rheological behavior of crystal-bearing magmas. Moreover, it is feasible that locally enhanced strain rates induce a transition to a power law melt rheology. In order to distinguish this effect from nonlinearities caused by crystal fracturing, it would be interesting to perform laboratory experiments in which the crystals have a significantly larger yield stress (e.g., by using corundum as a crystal phase). There have been a number of recent experiments in which evidence was found that crystals fracture during deformation [*Arbaret et al.*, 2007; *Champallier et al.*, 2008], although the consequences of this on the rheology of the suspension were not extensively studied.

6. Conclusions

[63] We developed a 0-D technique to determine the effective viscosity of a crystal-melt assemblage that employs the full stress-strain curve. Applying this method to recently published laboratory experiments confirms earlier findings that adding crystals to magma causes the rheology to be strongly strain rate dependent, with power law coefficients as large as $n = 13$.

[64] Several processes have recently been suggested to be responsible for this nonlinearity, which includes finite strain effects (reordering of crystals), shear heating, power law melt (nonlinear viscous melt) rheology and plastic failure of crystals. In order to assess the relative importance of each of these effects we have performed 2-D direct numerical simulations on both synthetic setups (with elliptical or spherical particles) as well as with a setup that was digitized from a laboratory experiment.

[65] Numerical simulations using parameters characteristic for laboratory experiments of *Caricchi et al.* [2007] indicate that shear heating as well crystal rearrangements have a minor effect. If the melt has a non-Newtonian rheology, the power law coefficient of the aggregate will exactly reflect that of the melt. This can thus potentially contribute to the nonlinear rheology of the assemblage, but it seems unlikely that it is the sole cause for the very large power law coefficients.

[66] The simulations also showed that stresses within a sample can locally be more then 15 times larger then average sample stresses recorded by stress-strain curves. Therefore, it is quite feasible that brittle (plastic) failure of crystals occurs during ongoing deformation. Our simulations indicated that

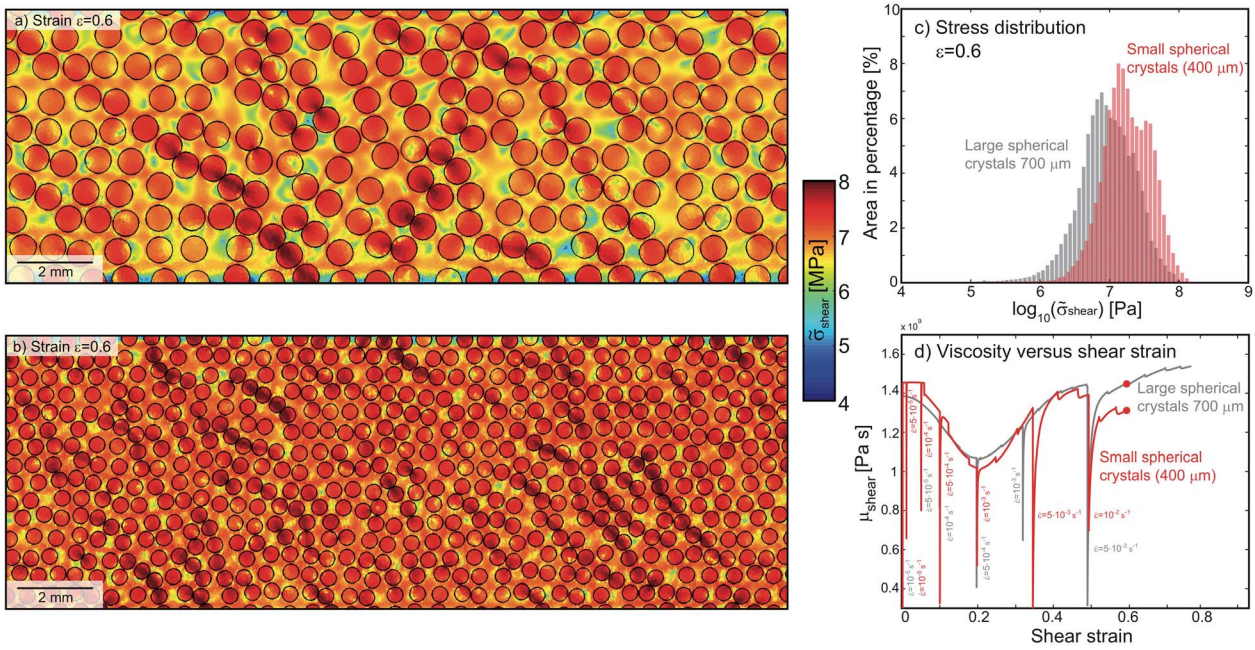

Figure B1. Stress distribution of simulations using Newtonian viscous rheology (model A) for (a) large crystals with diameter 700 mm and (b) 400 mm. (c) Stress distribution at $e = 0.6$ for the two different grain sizes. (d) Viscosity versus shear strain indicating strain rate steps and strain at which the stress distributions are shown.

this has a pronounced effect on the power law coefficient of the aggregate (which results in values as large as $n = 50$ in some cases). We thus conclude that plasticity is the dominant effect responsible for the strongly non-Newtonian behavior of crystal-melt systems that is observed in some laboratory experiments.

Appendix A: Definition of the Power Law Coefficient

[67] The rheological creep behavior of solid rocks on geological time scales can generally be described with an equation of the form

$$\sigma^n = A\dot{\varepsilon}, \tag{A1}$$

where σ is stress, $\dot{\varepsilon}$ strain rate, A a material parameter and n the power law coefficient [e.g., *Ranalli*, 1995]. In most quantitative geodynamic models, a different form of this expression is used:

$$\sigma = A^{\frac{1}{n}}\dot{\varepsilon}^{\frac{1}{n}} = \mu_{eff}\dot{\varepsilon}, \tag{A2}$$

where $\mu_{eff} = A^{\frac{1}{n}}\dot{\varepsilon}^{\frac{1}{n}-1}$ is the effective viscosity [e.g., *Gerya*, 2010]. If solid rocks deform in the diffusion creep regime, $n = 1$ and the effective viscosity is independent of the applied strain rate, which is also known as linear or Newtonian viscous creep. In the dislocation creep regime, $n > 1$ (typically $n \approx 3$–4) and the viscosity decreases with increasing strain rate, which is a non-Newtonian behavior.

[68] For the analysis presented in this paper we consistently use the form given in equation (A2) and the power law coefficient n in the text is always referring to the n as given in the equation.

Appendix B: Influence of Particle Size

[69] The influence of particle size is tested by two forward simulations with different particle sizes but the same solid fraction of $\phi_s = 0.5$. Sizes of 700 μm and 400 μm are employed which correspond to 3.5% and 2% of the total domain width $W = 19$ mm (Figure B1). The resulting aggregate stresses of both crystal sizes show very similar distributions below strains for strains smaller then 0.5, but behave slightly different for larger strains (Figure B1c). However, this discrepancy is most likely due to the fact that strain rate steps were performed at slightly different strains (Figure B1d).

Acknowledgments

[70] This work was supported by the Swiss National Science Foundation grant 200021-107889. BK was partly supported by the European Research Council with ERC grant agreement 258830.

References

Arbaret, L., M. Bystricky, and R. Champallier (2007), Microstructures and rheology of hydrous synthetic magmatic suspensions deformed in torsion at high pressure, *J. Geophys. Res.*, *112*, B10208, doi:10.1029/2006JB004856.

Arzi, A. A. (1978), Critical phenomena in rheology of partially melted rocks, *Tectonophysics*, *44*(1–4), 173–184, doi:10.1016/0040-1951(78)90069-0.

Bagdassarov, N.S., D. B. Dingwell, and S. L. Webb (1994), Viscoelasticity of crystal-bearing and bubble-bearing rhyolite melts, *Phys. Earth Planet. Inter.*, *83*(2), 83–99, doi:10.1016/0031-9201(94)90066-3.

Caricchi, L., L. Burlini, P. Ulmer, T. Gerya, M. Vassalli, and P. Papale (2007), Non-Newtonian rheology of crystal-bearing magmas and implications for magma ascent dynamics, *Earth Planet. Sci. Lett.*, *264*(3–4), 402–419, doi:10.1016/j.epsl.2007.09.032.

Champallier, R., M. Bystricky, and L. Arbaret (2008), Experimental investigation of magma rheology at 300 MPa: From pure hydrous melt to 76 vol.% of crystals, *Earth Planet. Sci. Lett.*, *267*(3–4), 571–583, doi:10.1016/j.epsl.2007.11.065.

Cleary, P. W. (2008), The effect of particle shape on simple shear flows, *Powder Technol.*, *179*(3), 144–163, doi:10.1016/j.powtec.2007.06.018.

Cordonnier, B., K.-U. Hess, Y. Lavallee, and D. B. Dingwell (2009), Rheological properties of dome lavas: Case study of Unzen volcano, *Earth Planet. Sci. Lett.*, *279*(3–4), 263–272, doi:10.1016/j.epsl.2009.01.014.

Costa, A. (2005), Viscosity of high crystal content melts: Dependence on solid fraction, *Geophys. Res. Lett.*, *32*, L22308, doi:10.1029/2005GL024303.

Costa, A., L. Caricchi, and N. Bagdassarov (2009), A model for the rheology of particle-bearing suspensions and partially molten rocks, *Geochem. Geophys. Geosyst.*, *10*, Q03010, doi:10.1029/2008GC002138.

Cuvelier, C., A. Segal, and A. van Steenhoven (1986), *Finite Element Methods and the Navier-Stokes Equations*, D. Reidel, Dordrecht, Netherlands.

Deubelbeiss, Y. (2010), Numerical modeling of particle suspensions with application to crystal-melt systems, Ph.D. thesis, 155 pp., Dep. of Earth Sci., ETH Zurich, Zurich, Switzerland.

Deubelbeiss, Y., and B. J. P. Kaus (2008), Comparison of Eulerian and Lagrangian numerical techniques for the Stokes equations in the presence of strongly varying viscosity, *Phys. Earth Planet. Inter.*, *171*(1–4), 92–111, doi:10.1016/j.pepi.2008.06.023.

Deubelbeiss, Y., B. J. P. Kaus, and J. A. D. Connolly (2010), Direct numerical simulation of two-phase flow: Effective rheology and flow patterns of particle suspensions, *Earth Planet. Sci. Lett.*, *290*(1–2), 1–12, doi:10.1016/j.epsl.2009.11.041.

Dingwell, D. B., and S. L. Webb (1990), Relaxation in silicate melts, *Eur. J. Mineral.*, *2*(4), 427–449.

Gerya, T. V. (2010), *Introduction to Numerical Geodynamic Modelling*, Cambridge Univ. Press, Cambridge, U. K.

Giordano, D., J. K. Russell, and D. B. Dingwell (2008), Viscosity of magmatic liquids: A model, *Earth Planet. Sci. Lett.*, *271*(1–4), 123–134, doi:10.1016/j.epsl.2008.03.038.

Hess, K. U., B. Cordonnier, Y. Lavallee, and D. B. Dingwell (2008), Viscous heating in rhyolite: An in situ experimental determination, *Earth Planet. Sci. Lett.*, *275*(1–2), 121–126, doi:10.1016/j.epsl.2008.08.014.

Kameda, M., H. Kuribara, and M. Ichihara (2008), Dominant time scale for brittle fragmentation of vesicular magma by decompression, *Geophys. Res. Lett.*, *35*, L14302, doi:10.1029/2008GL034530.

Kaus, B. J. P. (2010), Factors that control the angle of shear bands in geodynamic numerical models of brittle deformation, *Tectonophysics*, *484*(1–4), 36–47, doi:10.1016/j.tecto.2009.08.042.

Kaus, B. J. P., and Y. Y. Podladchikov (2006), Initiation of localized shear zones in viscoelastoplastic rocks, *J. Geophys. Res.*, *111*, B04412, doi:10.1029/2005JB003652.

Lagarias, J. C., J. A. Reeds, M. H. Wright, and P. E. Wright (1998), Convergence properties of the Nelder-Mead simplex method in low dimensions, *SIAM J. Optim.*, *9*(1), 112–147, doi:10.1137/S1052623496303470.

Lavallée, Y., K.-U. Hess, B. Cordonnier, and D. B. Dingwell (2007), Non-Newtonian rheological law for highly crystalline dome lavas, *Geology*, *35*(9), 843–846, doi:10.1130/G23594A.1.

Lavallée, Y., P. G. Meredith, D. B. Dingwell, K.-U. Hess, J. Wassermann, B. Cordonnier, A. Gerik, and J. H. Kruhl (2008), Seismogenic lavas and explosive eruption forecasting, *Nature*, *453*(7194), 507–510, doi:10.1038/nature06980.

Lejeune, A. M., and P. Richet (1995), Rheology of crystal-bearing silicate melts: An experimental study at high viscosities, *J. Geophys. Res.*, *100*, 4215–4229, doi:10.1029/94JB02985.

Moresi, L., S. Quenette, V. Lemiale, C. Meriaux, B. Appelbe, and H.-B. Muhlhaus (2007), Computational approaches to studying non-linear dynamics of the crust and mantle, *Phys. Earth Planet. Inter.*, *163*, 69–82, doi:10.1016/j.pepi.2007.06.009.

Morgan, J. K., and M. S. Boettcher (1999), Numerical simulations of granular shear zones using the distinct element method: 1. Shear zone kinematics and the micromechanics of localization, *J. Geophys. Res.*, *104*, 2703–2719, doi:10.1029/1998JB900056.

Mueller, S., E. W. Llewellin, and H. M. Mader (2010), The rheology of suspensions of solid particles, *Proc. R. Soc. A*, *466*(2116), 1201–1228, doi:10.1098/rspa.2009.0445.

Paterson, M. S., and D. L. Olgaard (2000), Rock deformation tests to large shear strains in torsion, *J. Struct. Geol.*, *22*(9), 1341–1358, doi:10.1016/S0191-8141(00)00042-0.

Petford, N. (2009), Which effective viscosity?, *Mineral. Mag.*, *73*(2), 167–191, doi:10.1180/minmag.2009.073.2.167.

Pinkerton, H., and R. J. Stevenson (1992), Methods of determining the rheological properties of magmas at sub-liquidus temperatures, *J. Volcanol. Geotherm. Res.*, *53*(1–4), 47–66, doi:10.1016/0377-0273(92)90073-M.

Ranalli, G. (1995), *Rheology of the Earth*, Chapman and Hall, London.

Roscoe, R. (1952), The viscosity of suspensions of rigid spheres, *Br. J. Appl. Phys.*, *3*(8), 267–269, doi:10.1088/0508-3443/3/8/306.

Rutgers, I. R. (1962), Relative viscosity of suspensions of rigid spheres in Newtonian liquids, *Rheol. Acta*, *2*, 202–210, doi:10.1007/BF01983952.

Saar, M. O., M. Manga, K. V. Cashman, and S. Fremouw (2001), Numerical models of the onset of yield strength in crystal-melt suspensions, *Earth Planet. Sci. Lett.*, *187*(3–4), 367–379, doi:10.1016/S0012-821X(01)00289-8.

Shewshuk, J. R. (1996), Triangle: Engineering a 2D quality mesh generator and Delaunay triangulator, in *Applied Computational Geometry: Towards Geometric Engineering*, *Lect. Notes Comput. Sci.*, vol. 1148, edited by M. C. Lin and D. Manocha, pp. 203–222, Springer, Berlin.

Stickel, J. J., and R. L. Powell (2005), Fluid mechanics and rheology of dense suspensions, *Annu. Rev. Fluid Mech.*, *37*, 129–149, doi:10.1146/annurev.fluid.36.050802.122132.

Völtz, C., M. Nitschke, L. Heymann, and I. Rehberg (2002), Thixotropy in macroscopic suspensions of spheres, *Phys. Rev. E*, *65*(5), 051402, doi:10.1103/PhysRevE.65.051402.

Webb, S. L., and D. B. Dingwell (1990a), Non-Newtonian rheology of igneous melts at high stresses and strain rates: Experimental results for rhyolite, andesite, basalt, and nepheline, *J. Geophys. Res.*, *95*, 15,695–15,701, doi:10.1029/JB095iB10p15695.

Webb, S. L., and D. B. Dingwell (1990b), The onset of non-Newtonian rheology of silicate melts. A fiber elongation study, *Phys. Chem. Miner.*, *17*(2), 125–132, doi:10.1007/BF00199663.